Article

Developmental Cell

Microtubules Negatively Regulate Insulin Secretion in Pancreatic β Cells

Highlights

- Microtubule disruption enhances glucose-stimulated insulin secretion
- Microtubules withdraw insulin granules from the cell periphery
- Glucose induces remodeling of Golgi-derived microtubules in β cells
- Microtubule meshwork is overly dense in β cells from diabetic mice

Authors

Xiaodong Zhu, Ruiying Hu, Marcela Brissova, ..., Alvin C. Powers, Guoqiang Gu, Irina Kaverina

Correspondence

guoqiang.gu@vanderbilt.edu (G.G.), irina.kaverina@vanderbilt.edu (I.K.)

In Brief

Zhu et al. examine the mechanism regulating availability of insulin granules for secretion in pancreatic β cells, showing that non-directional vesicular transport along Golgi-derived microtubules limits granule dwelling at the cell periphery. Consistently, microtubule depolymerization facilitates secretion in vitro and in mice and glucose stimuli remodel microtubules to control secretion.

Zhu et al., 2015, Developmental Cell *34*, 656–668
September 28, 2015
http://dx.doi.org/10.1016/j.devcel.2015.08.020

CellPress

CellPress

Developmental Cell
Article

Microtubules Negatively Regulate Insulin Secretion in Pancreatic β Cells

Xiaodong Zhu,[1] Ruiying Hu,[1] Marcela Brissova,[2] Roland W. Stein,[1,3] Alvin C. Powers,[2,3,4] Guoqiang Gu,[1,*] and Irina Kaverina[1,*]

[1]Department of Cell and Developmental Biology, Vanderbilt University Medical Center, Nashville, TN 37240, USA
[2]Division of Diabetes, Endocrinology, and Metabolism, Department of Medicine, Vanderbilt University Medical Center, Nashville, TN 37232, USA
[3]Department of Molecular Physiology and Biophysics, Vanderbilt University Medical Center, Nashville, TN 37232, USA
[4]VA Tennessee Valley Healthcare System, Nashville, TN 37212, USA
*Correspondence: guoqiang.gu@vanderbilt.edu (G.G.), irina.kaverina@vanderbilt.edu (I.K.)
http://dx.doi.org/10.1016/j.devcel.2015.08.020

SUMMARY

For glucose-stimulated insulin secretion (GSIS), insulin granules have to be localized close to the plasma membrane. The role of microtubule-dependent transport in granule positioning and GSIS has been debated. Here, we report that microtubules, counterintuitively, restrict granule availability for secretion. In β cells, microtubules originate at the Golgi and form a dense non-radial meshwork. Non-directional transport along these microtubules limits granule dwelling at the cell periphery, restricting granule availability for secretion. High glucose destabilizes microtubules, decreasing their density; such local microtubule depolymerization is necessary for GSIS, likely because granule withdrawal from the cell periphery becomes inefficient. Consistently, microtubule depolymerization by nocodazole blocks granule withdrawal, increases their concentration at exocytic sites, and dramatically enhances GSIS in vitro and in mice. Furthermore, glucose-driven MT destabilization is balanced by new microtubule formation, which likely prevents over-secretion. Importantly, microtubule density is greater in dysfunctional β cells of diabetic mice.

INTRODUCTION

Glucose-stimulated insulin secretion (GSIS) in pancreatic β cells maintains glucose homeostasis and prevents diabetes. Despite decades of studies, our knowledge about what controls the precise amount of insulin release on a given stimulus is incomplete. Each β cell has over 10,000 secretory vesicles containing insulin (also known as dense core granules or insulin granules) (Dean, 1973; Olofsson et al., 2002); yet sustained high glucose exposure only releases several hundred granules, suggesting that specific mechanisms regulate the releasability of most granules (Rorsman and Renström, 2003).

A key mechanism that restricts insulin secretion is controlling the number of insulin granules located in the proximity of the plasma membrane, which is a net result from the delivery of granules to the plasma membrane and their withdrawal back to the cell interior. It is thought that microtubules (MTs), 25 nm-thick dynamic cytoskeletal polymers of α/β tubulin dimers, play an essential role in insulin granule positioning. In 1968, Lacy et al. (1968) proposed that MTs are involved in insulin granule linkage to sites of secretion at the plasma membrane. Thereafter, several studies suggested that disrupting MTs in β cells disturbed GSIS (Malaisse et al., 1974; Suprenant and Dentler, 1982). Brinkley's group, who studied insulin secretion using disseminated cell culture from the whole pancreas, proposed a model whereby insulin granules residing in the cell interior are transported toward secretion sites along radial MT arrays (Boyd et al., 1982). This model appears plausible, because in many cell types long-distance secretory membrane trafficking utilizes MT tracks, which extend radially from the cell center to the periphery. However, while MT-dependent motors indeed continuously translocate insulin granules along MTs (Heaslip et al., 2014; Varadi et al., 2002, 2003), the radial MT tracks reported in pancreatic cells by Boyd et al. (1982) were not confirmed by later studies: in β-cell lines MTs form a complex non-directional mesh (Heaslip et al., 2014; Varadi et al., 2002), poising challenges for directional cargo transport. Furthermore, the importance of MTs for GSIS has been questioned by recent experimental (Mourad et al., 2011) and computational (Tabei et al., 2013) studies, which showed that MTs are not required for GSIS and that random, diffusion-like movement rather than directional transport accounts for vesicular delivery in β cells, respectively.

MT-dependent insulin granule transport has been best studied utilizing total internal reflection fluorescence (TIRF) microscopy in β-cell culture models (Heaslip et al., 2014; Hoboth et al., 2015; Varadi et al., 2003). It has become clear that recently generated ("young") insulin granules, competent of release, are moved along the cell membrane in a MT-dependent manner (Hoboth et al., 2015). Such lateral insulin granule transport is driven by the interplay of MT plus end-directed kinesin-1 and MT minus end-directed cytoplasmic dynein (Varadi et al., 2002, 2003). Unfortunately, because TIRF only visualizes granule movement parallel to the plasma membrane, the full role of MT in the movement of insulin granules from the cell center to the cell periphery is still unclear.

Several technical challenges hinder the analysis of MT structure-function relationships in β cells. On one hand, analysis

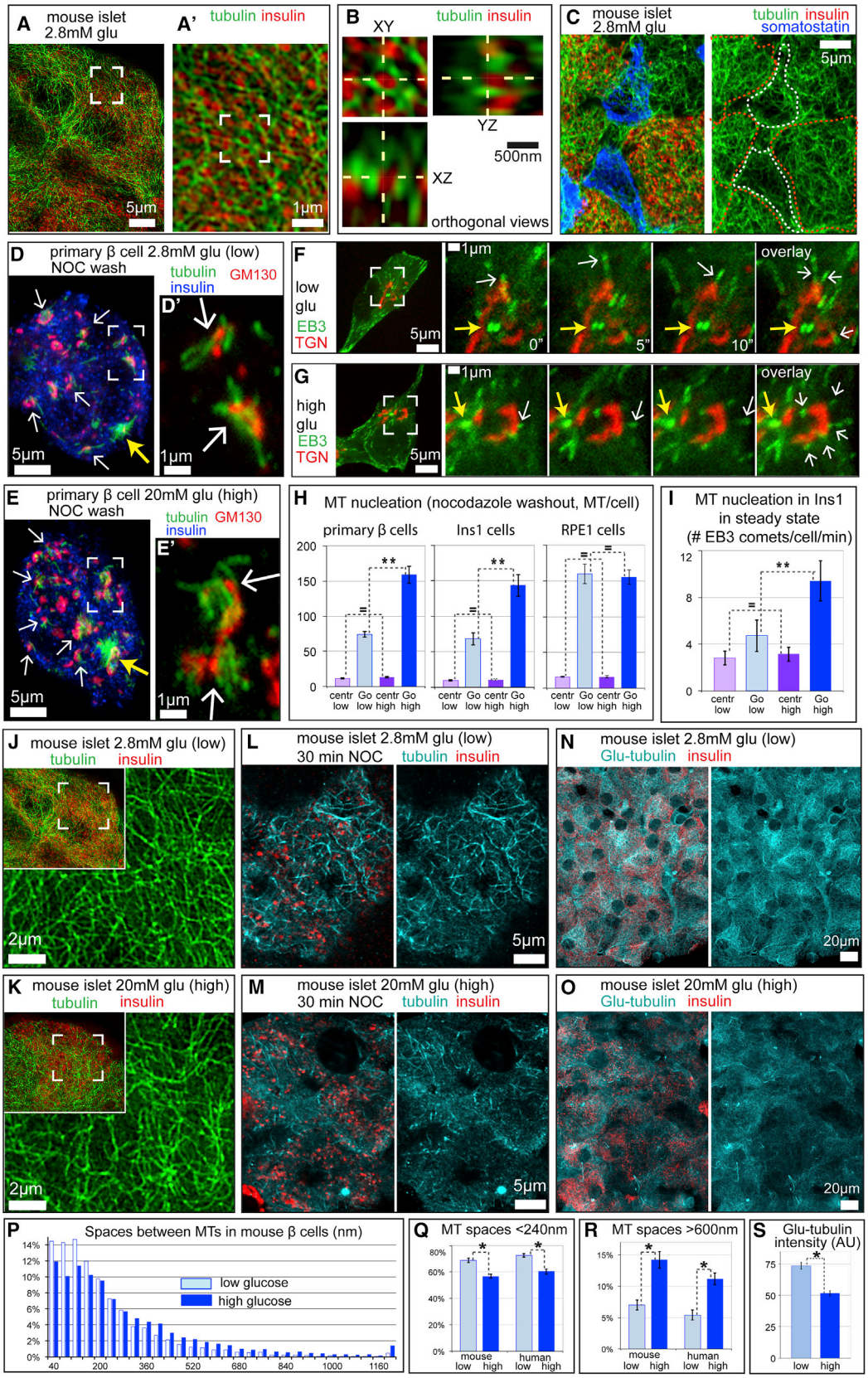

(legend on next page)

of complex MT organization and dynamics requires modern high- and super-resolution microscopy, which have limited capacities in resolving thick samples, such as intact islets. On the other hand, dissociated primary β cells rapidly de-differentiate in culture and cultured β-cell lines usually have compromised GSIS. This precludes most thorough microscopy studies from direct assessment of MT function in GSIS in functional β cells and raises concerns that altered MT structure and regulatability may accompany β-cell de-differentiation.

Taking into account our findings on Golgi-derived MTs in secretory cells (Efimov et al., 2007), we revisit MT structure and function in insulin secretion, analyzing intact pancreatic islets by high- and super-resolution microscopy, in combination with direct detection of in vitro and in vivo GSIS. We uncover a surprising, yet critical, MT function in β cells in precisely controlling GSIS and suggest that disturbance of this control may contribute to β-cell dysfunction in type 2 diabetes mellitus.

RESULTS

Differentiated β Cells Contain Dense MT Meshwork Derived from the Golgi Complex

Because MTs serve as tracks for intracellular trafficking, spatial organization of MTs underlies their cellular function. To analyze the 3D MT network in functional β cells within murine pancreatic islets, we applied super-resolution structural illumination microscopy (SIM), which allows for the optical resolution up to 100 nm. β-cell MTs comprise a multi-directional, mesh-like network (Figures 1A and 1A'), similar to that in MIN6 β cells (Varadi et al., 2003). Insulin granules (~3–400 nm in diameter, see Olofsson et al., 2002) were often observed constrained within the openings of the MT network (Figure 1B), which had average spacing of 484 ± 40 nm. Such high MT density was predominantly observed in β cells, but not δ cells (Figure 1C), suggesting that dense MT meshwork is typical for β cells. Such MT organization is remarkably different from that of most other cell types, where MTs are nucleated at the centrosome-based MT-organizing center (MTOC) and extend to the cell periphery in a radial fashion (Alberts et al., 2002).

To understand how this unusual MT configuration arises, we analyzed MT nucleation in primary β cells by nocodazole washout assays. After complete MT depolymerization by nocodazole, the drug was removed and sites of de novo MT formation were detected. Interestingly, the number of MTs found at the centrosome was relatively low; instead, the majority of MTs in β cells emerged from the Golgi complex (Figures 1D, 1E, and 1H and Movie S1). This finding was confirmed by live-cell imaging of new MT formation in non-treated (steady-state) INS-1 cells (Figures 1F, 1G, and 1I), indicating that the Golgi acts as the major MTOC in pancreatic β cells.

Glucose Regulates MT Nucleation and Dynamics in β Cells

To address whether the unique MT organization in β cells contributes to their response to glucose, we tested whether glucose stimulation affects the MT network. Strikingly, high glucose dramatically enhances new MT nucleation from the Golgi, but not the centrosome (Figures 1E and 1G–1I and Movies S2 and S3). Importantly, this effect was specific for β cells, since it was observed in both primary β cells and INS-1 cells, but not retinal pigment epithelial cells (RPE1) (Figure 1H), which also contain Golgi-derived MTs (Efimov et al., 2007).

Unexpectedly, the glucose-enhanced MT nucleation did not lead to increased MT density in β cells, in either murine or human islets (Figures 1J, 1K, S1A, and S1B). In fact, high glucose decreased MT density: fewer small MT mesh openings (diameter <240 nm) and more large MT mesh openings (>600 nm) were detected under high glucose conditions (Figures 1P–1R and S1C). This result suggests that high glucose induces depolymerization of pre-existing MTs simultaneously with the MT nucleation boost. Indeed, high glucose treatment

Figure 1. Dynamics of Dense Golgi-Derived MT Network in Pancreatic β Cells Are Facilitated by Glucose

(A and B) SIM images of murine islet β cells at 2.8 mM glucose, insulin (red) and tubulin (green). The box from (A) is enlarged in (A'). The insulin granules are constrained between MTs, as shown in (B) by orthogonal views of the boxed area from (A).

(C) Confocal image of murine islet. The MTs in β cells (red outlines) are denser than in δ cells (white outlines), insulin (red), tubulin (green), and somatostatin (blue).

(D–E') Immunostained primary β cells (insulin, blue) 90 s after nocodazole washout at 2.8 mM (D) or 20 mM (E) glucose. The white arrows show MTs (tubulin, green) nucleated from the Golgi mini-stacks (GM130, red). The centrosome-nucleated MT asters are shown by yellow arrows in the image. The MT and Golgi from boxes in (D) and (E) are zoomed in (D') and (E'). See also Movie S1.

(F and G) Live-cell confocal imaging of INS-1 cells at 3 mM (F) or 20 mM (G) glucose. The boxes for whole cell overviews (left) are enlarged as time frames (right). The multiple MT plus ends (EB3-GFP, green) extend from the Golgi (RFP-TGN, red, shown by white arrows) and few MTs grow from the centrosome (GFP-centrin, green, shown by yellow arrows). See also Movies S2 and S3.

(H) High glucose (20 mM) stimulates MT nucleation from the Golgi in primary β cells (n = 7–10) and INS-1 (n = 11–13), but not RPE1 (n = 8) (asterisks, $p < 0.0001$.)

(I) Steady-state MT nucleation at the Golgi is significantly enhanced by 2.8 mM to 20 mM glucose switch (asterisks, $p < 0.05$) (n = 7–11) (based on data as in F and G).

(J and K) SIM images of MT organization in murine islet β cells at 2.8 mM (J) and 20 mM glucose (K). The MT images are zoomed from boxes in overviews (upper right corner) (insulin, red and tubulin, green).

(L and M) Confocal images of stable MTs remaining after short 30 min nocodazole treatment in 2.8 mM glucose (L) or 20 mM glucose (M) in murine islet β cells (insulin, red and tubulin, cyan).

(N and O) Confocal images of immunostained Glu-tubulin at 2.8 mM glucose (N) and 20 mM glucose (O) in murine islet β cells (insulin, red and Glu-tubulin, cyan).

(P) Histogram distribution of spaces between MTs at low (2.8 mM) or high (20 mM) glucose conditions for mouse islet β cells (n = 5,490–5,503 spaces from 23–26 cells) (based on SIM images).

(Q) High glucose decreases tight MT spacing in both human and mouse islet β cells (asterisks, $p < 0.0001$) (n = 17–26 cells).

(R) High glucose increases large MT spacing in both human and mouse islet β cells (asterisks, $p < 0.0001$) (n = 17–26 cells).

(S) Fluorescence intensity of immunostained Glu-tubulin (as in N and O) is decreased in high glucose (asterisks, $p < 0.0001$) (n = 68–77 cells) (based on data as in N and O). In (H), (I), and (Q)–(S), mean ± SEM are shown.

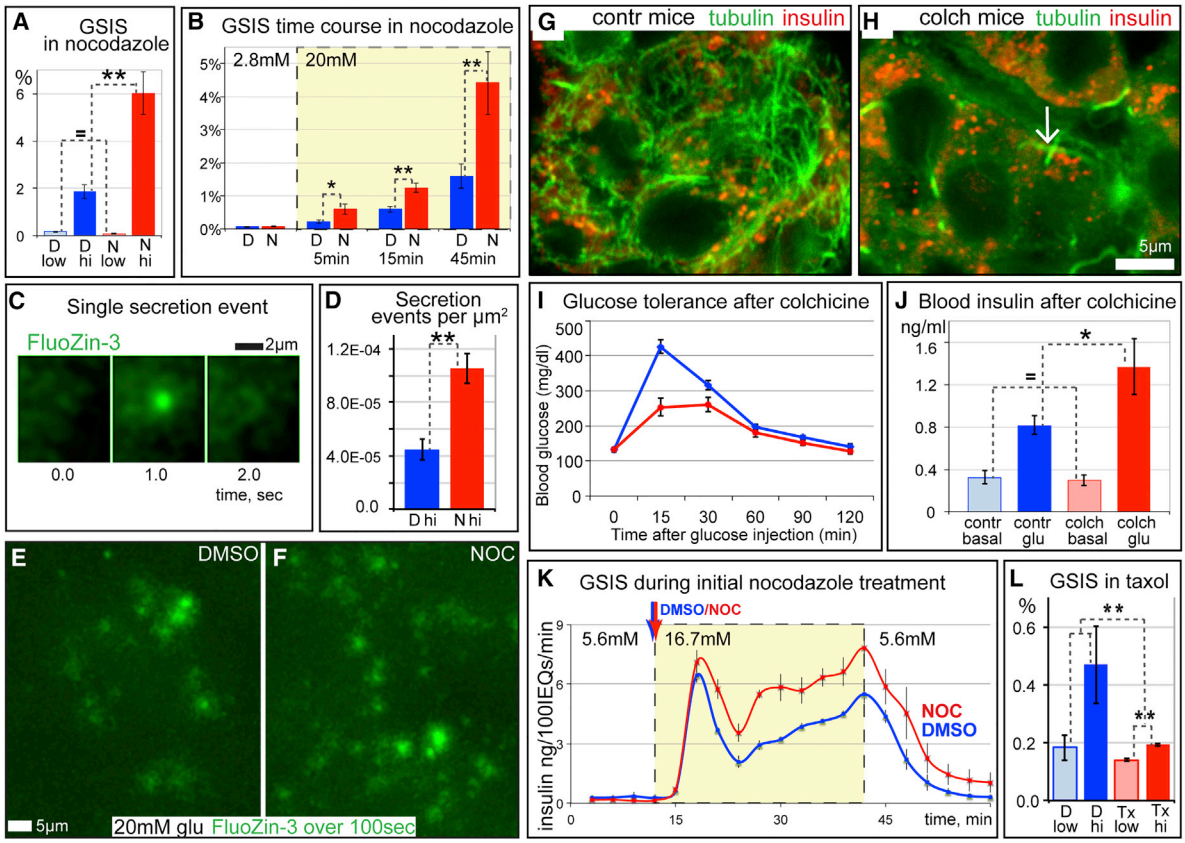

Figure 2. MT Depolymerization Enhances and MT Stabilization Blocks GSIS

(A) Static GSIS over 45 min in nocodazole (red) or DMSO (blue) pre-treated islets. The glucose concentrations of 2.8 mM (low) or 20 mM (high) are shown (asterisks, $p < 0.005$) (equals sign, $p > 0.5$) (n = 6 experiments). Here and below, static GSIS is shown as the percent of total insulin content after 45 min of treatment, which did not differ between DMSO and drug-treated islets (Table S1).

(B) Time course of GSIS in nocodazole (red) or DMSO (blue) pre-treated islets (asterisk, $p < 0.05$) (double asterisks, $p < 0.01$) (n = 8 experiments). The mean ± SEM are shown.

(C) A representative sequence illustration of a single secretion event. Note that a FluoZIn-3 signal is detected in a single frame.

(D) Secretion events quantified as FluoZin-3 fluorescence flashes in TIRF microscopy field in intact flattened islets in high glucose. The number of events per frame per μm^2 is shown as mean ± SEM ($p < 0.005$) (n = 5 islets) (based on data as in Movie S4).

(E and F) Maximal intensity projection overlays of FluoZin-3 imaging sequences over 100 s. The frequency of secretion events is strongly enhanced in nocodazole (F) and compared to DMSO (E). See also Movie S4.

(G and H) Confocal images of immunostained pancreatic tissue sections from mice subjected to control (G) and colchicine (H) injections (tubulin, green and insulin, red). The MTs are significantly destroyed in colchicine-injected mice (H) (arrow, primary cilia).

(I) Glucose tolerance in mice is improved after colchicine injection.

(J) Serum insulin content after glucose stimulus is increased after colchicine injection.

(I and J) Mean ± SEM are shown (n = 16 mice).

(K) GSIS after initial MT destabilization measured by perfusion with pancreatic islets. The nocodazole (5 μg/ml, red) or DMSO (blue) was added together with high glucose (n = 4 experiments).

(L) Static GSIS over 45 min in taxol (red) or DMSO (blue) pre-treated islets. The glucose concentration of 2.8 mM (low) or 20 mM (high) is shown (asterisks, $p < 0.05$) (n = 6 experiments). The mean ± SEM are shown.

decreased both MT resistance to the MT-depolymerizing drug nocodazole (Figures 1L and 1M) and tubulin detyrosination (a post-translational modification indicative of long MT lifetime, see Janke and Bulinski, 2011) (Figures 1N, 1O, and 1S). This means that MTs in glucose-stimulated β cells are short-lived and must be replaced by newly polymerized MTs to maintain the MT network. We conclude from these data that MT dynamic turnover, which includes both polymerization and depolymerization of MTs, is triggered by increased glucose.

MT Depolymerization Facilitates GSIS In Vitro and In Vivo

Our finding that MTs dynamics responds to glucose, led us to revisit the role of MTs in GSIS from whole islets, in which MTs have been depolymerized by nocodazole (Figures S1D–S1G). Surprisingly, complete MT disruption by 2 hr pre-incubation in nocodazole strongly increased islet GSIS, but did not alter basal insulin secretion (Figures 2A and 2B). This effect was specific for β cells since somatostatin secretion from δ cells was not enhanced in nocodazole-pre-treated islets (Figure S2A).

To test whether detected insulin content in the medium correlates with the secretion rate rather than non-specific effects (e.g., cell lysis), we used FluoZin-3, a cell-impermeable dye that becomes instantly fluorescent upon Zn^{2+}-binding, and is used to detect secretion of Zn^{2+}-rich insulin granules (Gee et al., 2002). To detect insulin secretion in intact live islets, we applied fast TIRF imaging to "flattened islet" cultures where robust GSIS was maintained (Supplemental Information) and recorded insulin secretion events, which manifested as peaks of FluoZin-3 fluorescence (Figure 2C). This approach showed a strong increase in secretion events in islets pre-treated with nocodazole (Figures 2D–2F and Movie S4; Table S2), indicating that MT depolymerization promotes GSIS via increased secretion activity.

We have further addressed the place of MT-dependent regulation within known physiological regulation of insulin secretion. MT regulation of GSIS proved not to be a part of the incretin-dependent pathway (Efendic and Portwood, 2004), since nocodazole further enhances GSIS after it has been potentiated by glucagon-like peptide (GLP-1, a major GSIS-amplifying gut hormone of the incretin group; Figure S2B). Indeed, the effects of high glucose on MT network density and stability were not influenced by GLP-1 (Figures S2C–S2M). Moreover, nocodazole significantly enhanced insulin secretion induced by arginine, KCl, tolbutamide, and IBMX (secretagogues that are known to stimulate insulin secretion via depolarizing β-cell membrane [arginine, KCl, tolbutamide] or via enhancing intracellular cyclic (c)AMP levels [IBMX]; see Sharp, 1979; Wollheim and Sharp, 1981; Figures S2N and S2O). These data indicate MT destabilization affect insulin secretion at distal regulatory steps, such as vesicle localization.

As a next step, we tested whether MT disruption in organisms has a physiologically significant effect on insulin secretion and blood glucose levels. We injected mice with colchicine, a less toxic MT-depolymerizing Food and Drug Administration (FDA)-approved drug, which disrupted MTs in tissues, including β cells (Figures 2G and 2H). This manipulation significantly improved glucose clearance in mice (Figure 2I) and enhanced levels of plasma insulin (Figure 2J), in agreement with the effect on isolated islets.

These data allowed us to conclude that MT depolymerization enhances GSIS, which bears significance in glucose homeostasis in vivo, and prompted a counterintuitive hypothesis that MTs restrict, rather than enhance, the number of insulin granules available for secretion. Interestingly, we found that even initial MT depolymerization as early as 5 min after nocodazole addition caused GSIS enhancement in experiments where nocodazole was added simultaneously with high glucose stimulation (Figure 2K). This suggests that insulin secretion is very sensitive to MT presence and partial MT depolymerization in frame of glucose-triggered MT destabilization (Figures 1J–1S) might increase the releasable insulin pool; if this is correct, blocking MT depolymerization must decrease GSIS. Consistent with this hypothesis, taxol-induced MT stabilization strongly inhibited GSIS (Figures 2L, S1H, and S1I), confirming published results (Howell et al., 1982; Mourad et al., 2011). This indicates that the capacity of MTs to depolymerize is a critical requirement for insulin secretion.

MTs Withdraw Insulin Granules from the Cell Membrane to Reduce Secretion

Because MT disruption enhances GSIS (Figure 2), we hypothesized that MTs prevent excessive secretion by withholding insulin granules or withdrawing them from the cell periphery.

To test this hypothesis, we visualized insulin granule behavior at the cell membrane in β cells within intact islets. The islets were derived from transgenic mice expressing an insulin-mCherry fusion protein specifically in β cells that did not interfere with β cell function (Figures S4A–S4D). Conveniently, insulin-mCherry was incorporated into insulin granules in a mosaic manner, highlighting a random subpopulation (approximately 7%) of granules that allowed for their easy tracking. Because TIRF optical sectioning visualizes the 200 nm-thick lowest cell's layer, it allowed us to analyze lateral granule movement parallel to the ventral cell membrane (Figures 3A–3D and Movies S5 and S6). We found that the majority of granules underwent minimal lateral displacements (<1 μm). Additionally, a subset of granules exhibited fast, randomly directed lateral movements, which were eliminated by nocodazole (Figure 3E), and thus were MT-dependent, consistent with the data from cell lines (Heaslip et al., 2014; Varadi et al., 2002).

Furthermore, TIRF experiments allowed us to analyze the dynamics of granule delivery to, and disappearance from, the cell periphery. Disappearance of granules from the TIRF field is likely due to a combination of secretion and withdrawal of granules back to the inner cytoplasm. However, insulin secretion is a rare event, although a substantial number of vesicles can be detected near the plasma membrane (Rorsman and Renström, 2003). Indeed, our quantification of the secretion events frequency using FluoZin-3 dye (Figures 2C–2E) showed that because insulin-mCherry highlights only a fraction of all insulin granules, the number of observed secretions of insulin-mCherry was extremely low (< 1.4 mCherry-labeled granules per min per movie). This allowed us to neglect the share of secretion in quantification of insulin-mCherry granule behavior and approximate that the insulin-mCherry granule disappearance represents granule withdrawal from the cell border.

Interestingly, we found that without glucose stimulation, the number of insulin-mCherry granules at the cell surface was constant both in control and MT-depleted cells. Also, when insulin secretion was stimulated in control cells, the overall number of granules in the TIRF field did not change (Figures 3F and 3H; Table S2), indicating that the number of granules delivered from the cell center was precisely balanced with the granules withdrawn (and secretion, to a lesser degree). In contrast, in islets pre-treated with nocodazole to eliminate MTs, the number of insulin granules in the TIRF field was dramatically and continuously increased (Figures 3G and 3H and Movie S6), indicating that the balance between insulin granule delivery and withdrawal was disturbed. Specifically, the share of granules disappearing from the field of view (as in Figures 3K and 3L) was reduced in nocodazole-treated cells as compared to control (Figure 3I), while granule delivery was unchanged (Figure 3J; Table S2). We conclude that, in the absence of MTs, granules fail to withdraw from the cell border; this leads to accumulation of insulin granules at the cell periphery and unregulated increase of the pool available for secretion. In contrast, normally, MTs provide a regulatory mechanism that balances the number of delivered and withdrawn granules.

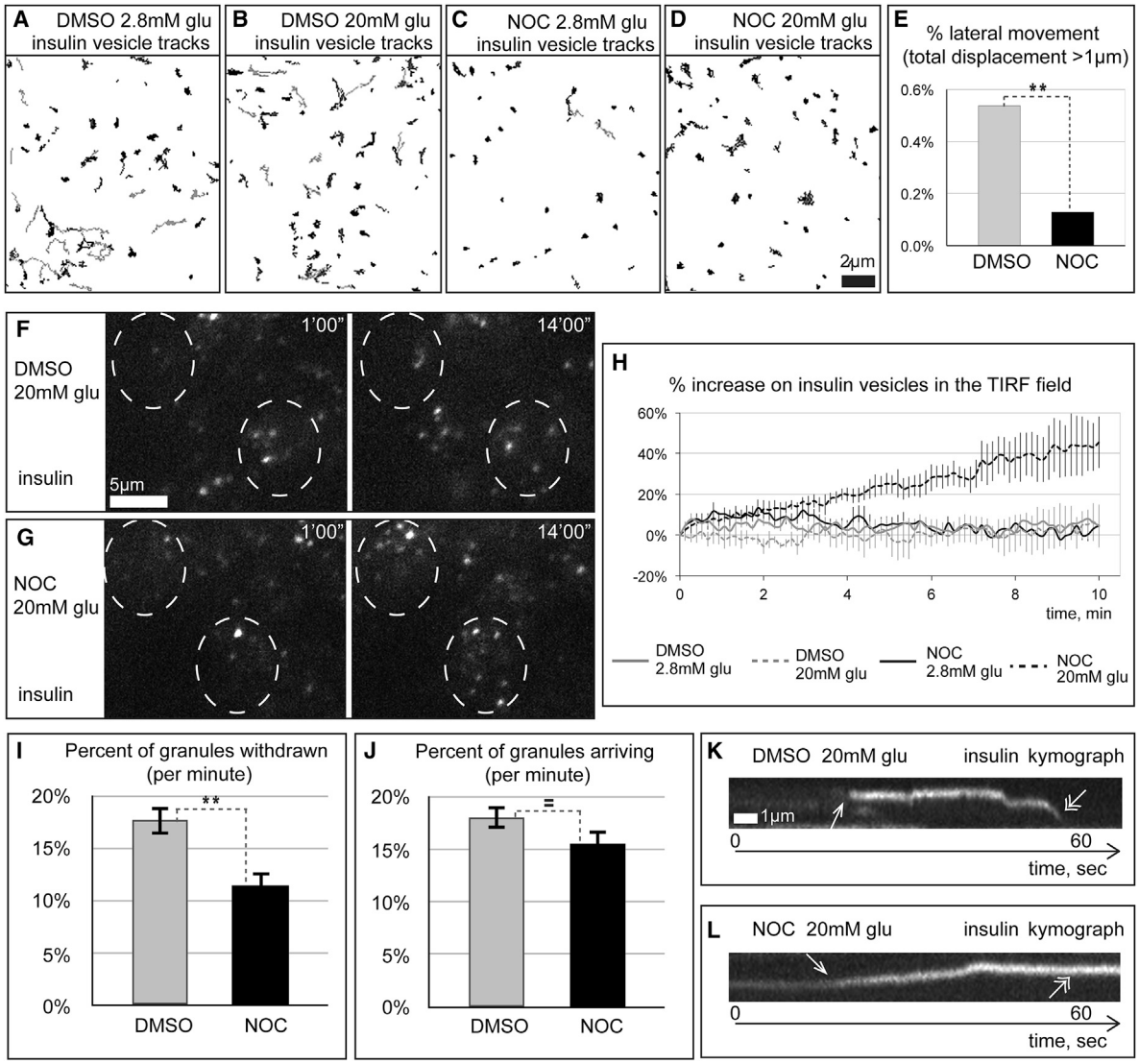

Figure 3. Lack of MTs during GSIS Interferes with Insulin Granule Withdrawal from the β-Cell Periphery

(A–D) Tracks of lateral insulin granule movement recorded by live TIRF microscopy of flattened *Rip*^{mCherry} islets in (A) DMSO + 2.8 mM glucose, (B) DMSO + 20 mM glucose, (C) nocodazole + 2.8 mM glucose, and (D) nocodazole + 20 mM glucose. The number of tracks with final displacement >0.77 μm (light gray) is decreased after nocodazole treatment. See also Movies S5 and S6.

(E) Long distance lateral movement of granules is blocked by nocodazole (2.8 mM glucose) (n = 5,494–6,230 tracks). The whole population percentage is shown (asterisks, $p < 0.0001$).

(F and G) Live TIRF microscopy of intact islets. The glucose stimulation does not change the number of mCherry-insulin granules in the TIRF field in DMSO (F, dotted circles), but dramatically increases it in nocodazole (G, dotted circles) (time after stimulation, min).

(H) Percent increase of insulin granules number in TIRF field under four conditions as in (A)–(D). Only nocodazole + 20 mM glucose leads to granule accumulation. The mean ± SEM are shown.

(I and J) Number of granules withdrawn from the TIRF field (I) within 1 min is decreased and number of granules delivered (J) is unchanged in nocodazole. The mean percentage ± SEM of insulin-mCherry-labeled granules in the field is shown (double asterisk, $p < 0.005$) (equal sign, $p > 0.1$) (n = 16 1-min movies from four islets).

(K and L) Representative kymographs (single-line intensity scans over time) of granules live in the TIRF field. In DMSO (K), granules are rapidly delivered to the membrane (acute appearance, single arrow) and withdrawn after a short dwelling period. Note that the withdrawal is accompanied with a lateral granule shift (double arrow). In nocodazole (L), granules are delivered by slow diffusion (slow signal increase, single arrow) and dwell at the membrane throughout the movie (double arrow) (time, s).

MT and Actin Cytoskeletons Cooperate to Control GSIS

The surprising stimulating effect of MT depolymerization on GSIS resembles the well-established reaction of β cells to actin cortex disassembly, which leads to dramatic enhancement of GSIS (Li et al., 1994; Thurmond et al., 2003; Wang and Thurmond, 2009). Because functional interplay of MT and actin cytoskeletons has been described in many cellular contexts (Goode et al., 2000), we tested whether MT depolymerization leads to

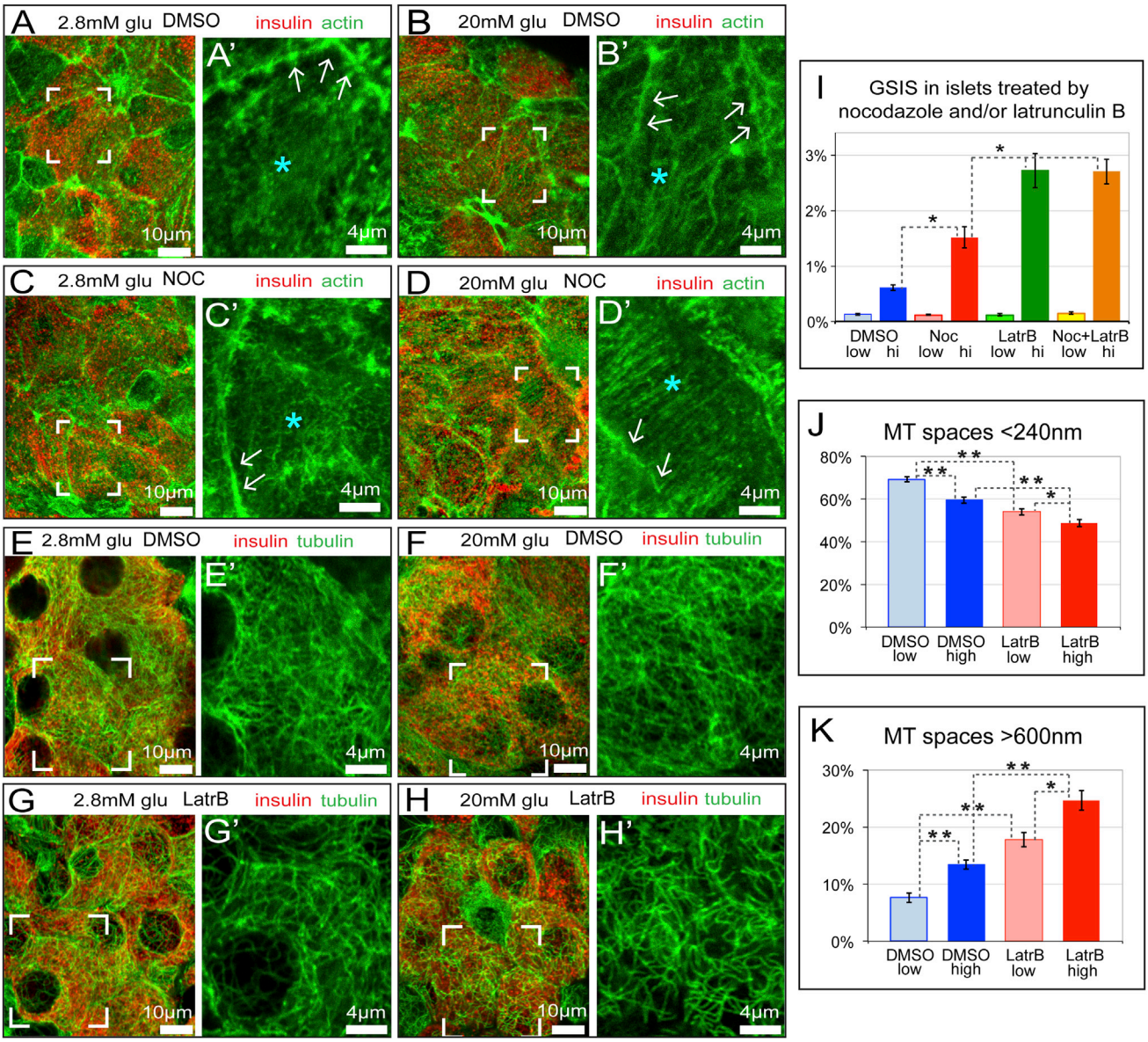

Figure 4. MTs and Actin Interplay to Regulate GSIS

(A–D') Confocal images of mouse islets immunostained for insulin (red) and actin (phalloidin, green) after nocodazole treatment. The actin images from boxes in (A)–(D) are zoomed in (A')–(D'). The intensity of the actin cortex at the cell borders (arrows) is diminished by high glucose (B' and D') as compared to low glucose (A' and C', respectively). The actin bundles in the cell interior (asterisks) are slightly increased in nocodazole treated cells (C' and D') as compared to DMSO (A' and B', respectively).

(E–H') Confocal images of mouse islets immunostained for insulin (red) and tubulin (green) after Latrunculin B treatment. The MT images from boxes in (E)–(H) are zoomed in (E')–(H'). The MT density is decreased by high glucose (F') and by Latrunculin B (G' and H').

(I) Static GSIS over 45 min in DMSO (blue), nocodazole (red), Latrunculin B (green), and nocodazole + Latrunculin B (yellow) pre-treated islets. The glucose concentrations of 2.8 mM (low) or 20 mM (high) are shown (asterisks, $p < 0.01$) ($n = 8$ experiments). The mean ± SEM are shown.

(J) Latrunculin B decreases tight MT spacing in mouse islet β cells at both low and high glucose levels (double asterisks, $p < 0.0001$) (asterisk, $p < 0.05$) ($n = 30–37$ cells).

(K) Latrunculin B increases large MT spacing in mouse islet β cells at both low and high glucose levels (double asterisks, $p < 0.0001$) (asterisk, $p < 0.01$) ($n = 30–37$ cells).

(J and K) Data are based on a histogram (data not shown) as in Figure 1P. The mean ± SEM are shown.

partial destruction of the actin cortex in β cells, providing a mechanism for GSIS enhancement. Nocodazole slightly enhanced actin bundling in the cytoplasm (Figures 4A–4D), which is not surprising given known activation of small GTPase RhoA downstream of MT depolymerization (Chang et al., 2008). However, we did not detect alterations in the actin cortex at the cell boundary in nocodazole- versus DMSO-treated islets under either low or high glucose conditions (Figures 4A–4D). We

concluded that it is unlikely that MT destabilization facilitates GSIS via actin cortex disassembly. Interestingly, further investigation of potential cytoskeletal crosstalk showed that actin depolymerization by Latrunculin B does cause significant loosening of the MT network (Figures 4E–4H'), to the level similar or above the loosening caused by the high glucose trigger (Figures 4J and 4K). Moreover, GSIS in Latrunculin B-treated islets was stronger than in nocodazole-treated islets and was not further enhanced by nocodazole (Figure 4I), suggesting that MT destabilization is one of the pathways that contributes to GSIS facilitation downstream of actin disruption. On the other hand, MT loosening in LatrunculinB-treated islets was further facilitated by high glucose (Figures 4J and 4K), indicating that physiological MT destabilization likely involves an additional, actin-independent mechanism.

Cytoskeleton-Driven Granule Transport Is Not Required for Insulin Secretion

Our data indicate that while MT disruption enhanced GSIS by blocking insulin granule withdrawal from the cell periphery, their delivery from the inner cytoplasm was unchanged. Disruption of the actin cytoskeleton also facilitates GSIS (Kalwat and Thurmond, 2013), raising a question whether cytoskeleton-dependent transportation of granules from the cell interior to the cell periphery is at all required for secretion. To address this, we followed 3D movement of granules in insulin-mCherry-expressing islets visualized by high-resolution confocal microscopy. Granule movement was subsequently analyzed by automatic tracking (Figures 5A–5I). Mean square displacement (MSD) analysis was used to analyze the whole granule population (Figure 5J); maximal track displacement of 0.4 μm and more was used to distinguish granules undergoing active transportation. We found that movement of insulin granules under all conditions was non-directional and fitted to the subdiffusion motion type (Saxton, 2007) (see Supplemental Information). In the absence of MTs, granules remained motile, indicative of an actin-dependent transportation mechanism. Indeed, in the absence of both cytoskeletal networks, granule displacement over 0.4 μm was a rare event.

The percentage of motile granules was increased by high glucose (Figure 5K). Interestingly, this increase was absent after MT disruption (Figure 5K), suggesting that glucose-driven regulation of transport requires MTs, which is consistent with previous findings (Donelan et al., 2002; Heaslip et al., 2014). Disruption of actin facilitated MT-dependent movement, but did not block glucose-dependent regulation of granule movement (Figure 5K).

These data agree with the previously proposed model where MTs and actin collaborate to drive non-directional insulin granule transport, based on observations in cell lines (Heaslip et al., 2014; Hoboth et al., 2015; Tabei et al., 2013); thus, these prior conclusions can be extrapolated into 3D granule transportation in intact islets. More importantly, we show that the ability of the cytoskeleton to displace granules does not correlate with high GSIS (Figure 4I). Rather, excessive secretion occurs when cytoskeletal elements are absent and/or loosened. We conclude that active transport of insulin granules is not required for GSIS and rather served for fine regulation of granule availability for secretion.

Overly Dense MTs in Dysfunctional β Cells Prevent Insulin Secretion

Our data indicate that the dense MT network in β cells acts to restrict GSIS, which means that unregulated increase in MT density might interfere with β-cell function in organisms. To determine whether alteration of the MT network is associated with diabetes, we compared dysfunctional β cells within pancreatic tissue sections from diabetic (*db*/*db*) mice (blood sugar > 350 mg/dl) with β cells of wild-type (WT) or healthy heterozygous control (*db*/+) mice by SIM. Strikingly, MTs in tissue sections (Figures 6A and 6B) and islets derived from *db*/*db* mice (Figure S5) were overly dense; the openings of the MT mesh were significantly smaller in *db*/*db* β cells than in controls (Figures 6C–6E). According to our model, abnormally high MT density reduces granule availability for release at the cell periphery. Indeed, after MT depolymerization by nocodazole, GSIS by *db*/*db* islets was significantly enhanced (Figure 6F), although not restored to WT levels. Vice versa, stabilization of MTs by taxol significantly decreased GSIS (Figure 6F), indicating that glucose-stimulated MT dynamics are required for insulin release from *db*/*db* β cells and that MT regulation of GSIS is still functional. We conclude that a pathway, which includes MT control of GSIS, is not blocked in this disease model; however, MT-dependent restriction of GSIS is overly active in *db*/*db* mice. It is possible that the elevated MT density arises as a protective mechanism to prevent depletion of insulin granules when β cells hyper-secrete insulin to counteract insulin resistance of *db*/*db* mice (Orland and Permutt, 1987) and serves as one of the mechanisms of disease progression.

DISCUSSION

The work presented here leads to a surprising conclusion that the major function of MT-based transport in β cells is to limit the number of insulin granules available for secretion on a given stimulus. The granule number at the cell periphery is controlled by constant removal of granules, moving along a non-directional MT network, regulated via glucose-dependent MT destabilization and Golgi-derived MT nucleation (Figure 7). Without MT control (in nocodazole), granules undergo excessive docking and secretion upon stimuli; in vivo, this over-secretion increases blood glucose clearance.

A main finding of our study is that physiological glucose destabilizes MTs in subcellular domains in β cells, resembling a local nocodazole effect. We hypothesize that such local MT depolymerization close to the plasma membrane creates a pool of MT-unattached granules, available for docking and secretion. Additional granule delivery is dispensable for this process, because insulin granules are abundant at the cell periphery, and only a small percentage is secreted on a given stimulus (Rorsman and Renström, 2003). While granule movement does not actively move toward the plasma membrane in the absence of MTs (Table S2), diffusion is sufficient for granule relocation to the docking sites. In the absence of MT-motor-driven withdrawal force, granules have sufficient time to be tethered and docked. As a result, MT destabilization becomes critical for GSIS and likely serves to precisely regulate secretion. This model incorporates the views that granule tethering/docking is an active glucose-dependent process that defines the number of

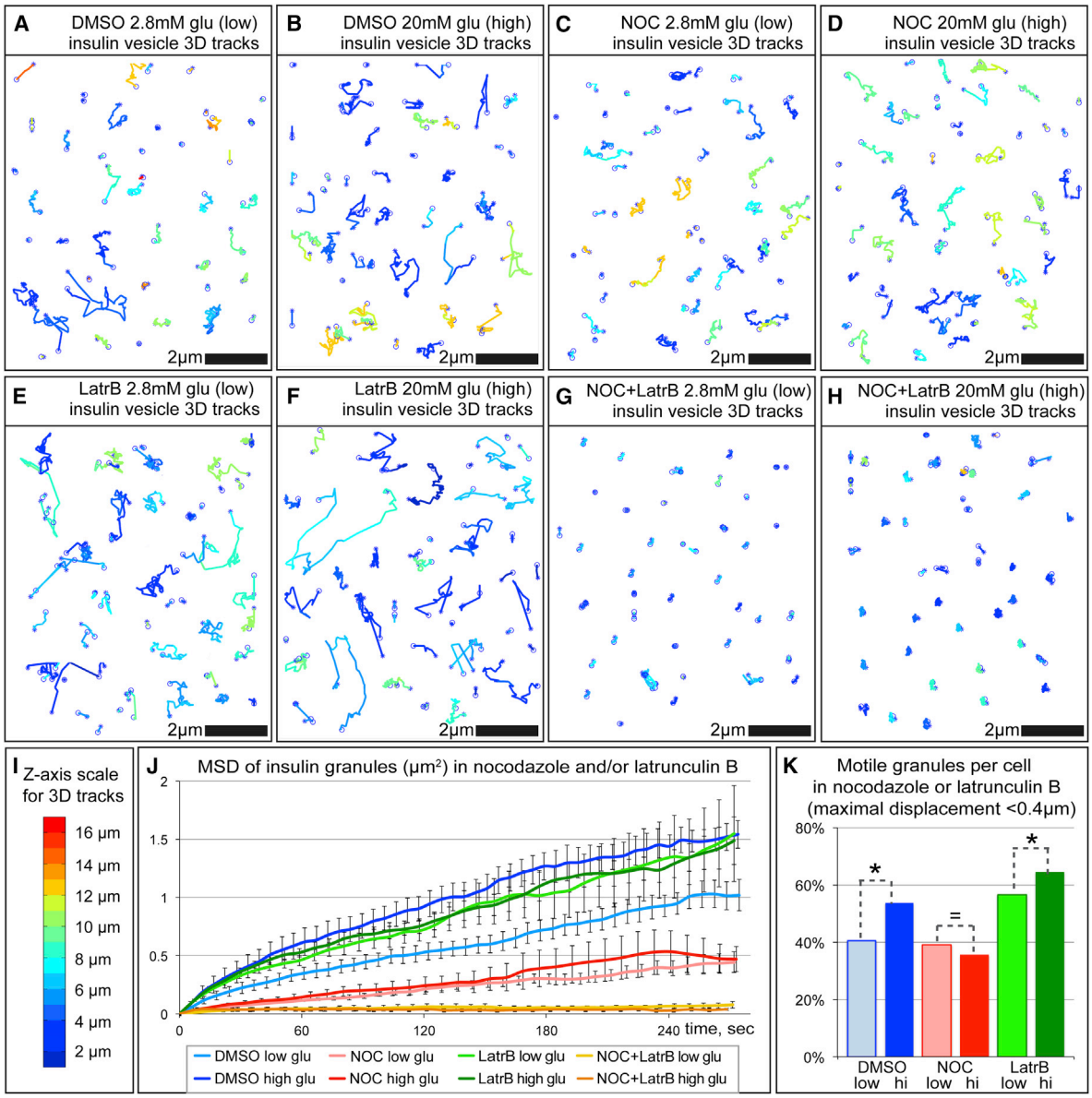

Figure 5. MTs and Actin Collaborate to Non-directionally Translocate Insulin Granules in Mouse Islets

(A–H) Examples of 3D movement tracks of mCherry-labeled insulin granules, recorded by spinning disk confocal microscopy. The pre-treatment: (A and B) DMSO, (C and D) nocodazole, (E and F) Latrunculin B, and (G and H) nocodazole + Latrunculin B. The glucose concentration: (A, C, E, and G) 2.8 mM (low) and (B, D, E, and H) 20 mM (high). The z axis is color coded as indicated in (I). See also Movies S7 and S8.

(J) MSD analysis of insulin dynamics at conditions as in (A)–(H). The insulin exhibits subdiffusion movement in all conditions. The movement velocity is dramatically decreased upon disruption of MTs (red) and even more so upon disruption of both MTs and actin (yellow) (n = 2,087–9,370 tracks from four islets). The mean ± SEM are shown.

(K) Percentage of motile granules (maximal 3D track displacement over 0.4 μm) upon disruption of the cytoskeleton. The glucose-dependent regulation of granule motility is not detected in nocodazole (n = 3,724–9,370 tracks). The whole population percentage is shown (asterisks, $p < 0.0001$) (equals sign, $p > 0.1$).

secretion-competent granules and requires a distinct (likely short) period when a granule is stationary in the vicinity of the docking machinery (Rorsman and Renström, 2003).

A critical requirement for efficient granule withdrawal from the secretion sites is a very dense MT network, which supports non-directional granule movement, or "random walk" (Tabei et al., 2013). Golgi-derived nucleation is a potent mechanism for such network formation, because the Golgi in β cells is relatively large and extends across a large part of the cytoplasm (Kanaani et al., 2015; Marsh et al., 2004; Sumara et al., 2009), providing multiple nucleation sites for a dense multi-directional MT network. Additionally, granules undergo non-directional movements switching between close tracks, which traps them in the β-cell interior. Glucose-dependent MT turnover in the cell center might remove restrain of trapped granules to contribute to GSIS enhancement. This function is similar to actin-dependent

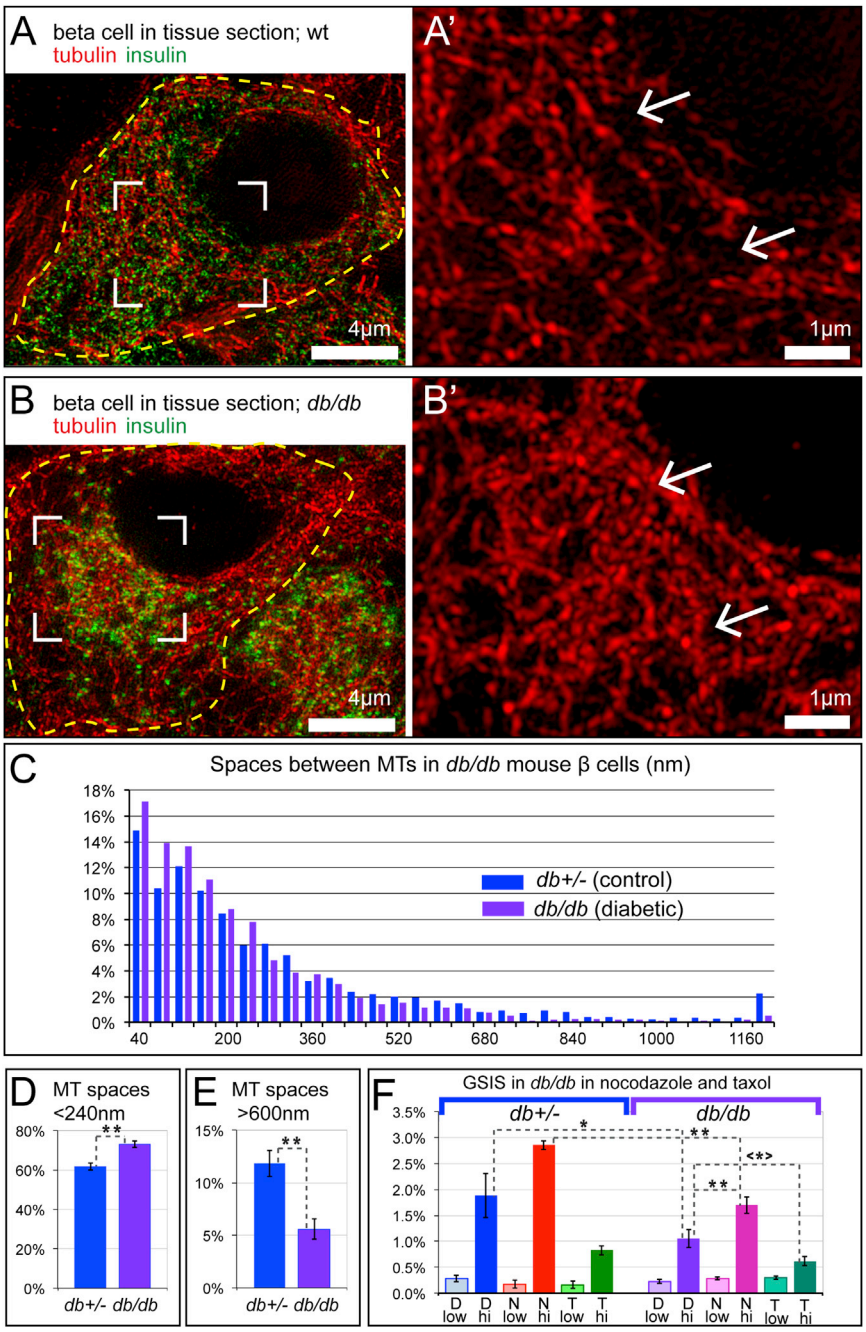

Figure 6. β-Cell MT Network Is Denser in *db/db* Mice Than in WT

(A–B') β cells in tissue sections from WT (A and A') and *db/db* mice (B and B'). SIM images are shown in the images. The yellow dashed lines indicate cell outlines. The MTs from boxes in (A) and (B) are zoomed in (A') and (B'). The arrows indicate typical MT spacing.

(C) Histogram distribution of spaces between MTs in β cells in *db*/+ and *db/db* islets (n = 1,972–2,303 spaces from 30 cells) (based on SIM images).

(D) Tight MT spacing is increased in β cells from *db/db* islets as compared to *db*/+ (asterisks, $p < 0.0001$) (n = 30 cells).

(E) Large MT spacing is decreased in β cells from *db/db* islets as compared to *db*/+ (asterisks, $p < 0.0001$) (n = 30 cells).

(F) Static GSIS over 45 min in DMSO, nocodazole, and taxol pre-treated islets from 4-month-old *db*/+ and *db/db* mice (n = 8–12 experiments). The glucose concentrations of 2.8 mM (low) or 20 mM (high) are shown (asterisk, $p < 0.05$) (double asterisk, $p < 0.01$) (bracketed asterisk, $p < 0.1$). In (D)–(F), mean ± SEM are shown.

restriction of transport described both for insulin granules (Heaslip et al., 2014; Hoboth et al., 2015) and pigment granules in melanocytes (Semenova et al., 2008; Wu et al., 1998). It is also clear that MTs tightly collaborate with the actin cytoskeleton to control insulin granule availability for secretion (Heaslip et al., 2014; Hoboth et al., 2015); here, we show that, as a part of this interplay, actin influences the density of MT network in β cells. This possibly occurs because MT ends can be stabilized by actin-dependent capture (Gundersen et al., 2004).

Importantly, we show that during GSIS, glucose-driven MT destabilization is balanced by new MTs formed at Golgi membranes, which likely prevents over-secretion of insulin. Along the same lines, MT plus end growth rates are increased under high glucose conditions in INS-1 cells (Heaslip et al., 2014). These data indicate that β-cell MTs play the role of cellular "rheostat", which is tuned according to physiological needs by modulating the density and dynamics of the MT meshwork, and precisely meters insulin release under a specific stimulus.

It is important to understand how facilitation of GSIS by reduction of MT density, reported here, is coordinated with the action of MT motors. Our, and previous observations (Tsuboi and Rutter, 2003; Varadi et al., 2003), indicate that both granule withdrawal into inner cytoplasm and lateral movements along the plasma membrane can move granules away from the secretion sites. In principle, movement of granules toward either MT end (e.g., kinesin-1 or dynein-driven, see Varadi et al., 2003) can either deliver or withdraw a granule from the secretion site because MT network in β cells lacks radial organization, and granules move chaotically. High glucose stimulus leads to activation of kinesin-1 (Donelan et al., 2002; McDonald et al., 2009) and MT-dependent granule movement. Our data suggest that more active movement should further restrict the time that granules spend at the docking sites where they are available for secretion. We hypothesize that in stimulated β cells where docking/priming of granules is strongly activated, over-secretion might occur without activation of MT-dependent withdrawal. On the other hand, depletion/inhibition of kinesin-1, as well as kinesin-1 knockout in mice, suppresses GSIS (Cui

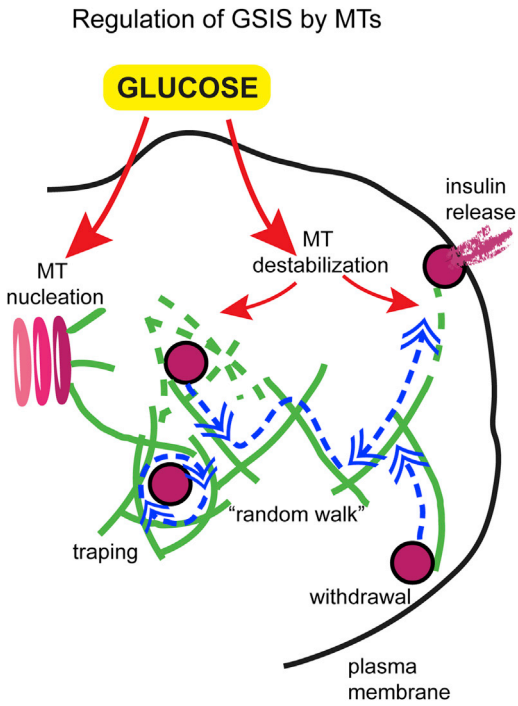

Figure 7. A Model of the Rheostat Function of MTs in β Cells

Dense MTs trap insulin granules in the cell center and promote their random walk. Non-directional granule movement leads to rapid granule withdrawal from the cell periphery, balanced with granule arrival. Glucose stimuli trigger both MT nucleation and destabilization. MT destabilization in the cell center reduces trapping. MT destabilization at the cell periphery decreases frequency of withdrawal and leads to free diffusion of detached granules, allowing for their docking. Enhanced MT nucleation at the Golgi balances MT destabilization, leading to fine rheostat regulation of granule availability for release.

et al., 2011; Donelan et al., 2002; McDonald et al., 2009; Meng et al., 1997). This might be explained by the presence of other molecular motors of the granule surface, which can hold granules at MTs when kinesin is blocked (Ally et al., 2009; Bryantseva and Zhapparova, 2012). In this case, granules would not become detached from MTs and available for secretion without kinesin-1. Indeed, inactivation of kinesin-1 has no effect on net localization of insulin granules within β cells (Cui et al., 2011).

While our findings and model are in line with recent findings describing MT motor-dependent transport of insulin granules (Heaslip et al., 2014; Hoboth et al., 2015; Tabei et al., 2013; Varadi et al., 2003), they do not agree with several previous studies showing decreased GSIS after MT disruption (Boyd et al., 1982; Malaisse et al., 1974; Suprenant and Dentler, 1982). Given the consistency of our observations ranging from single cells to whole animals, such discrepancy can be potentially explained by the variability in the experimental conditions for islet isolation, in vitro culture, and insulin GSIS assay, which could have resulted in variable MT reconfiguration and vesicular localization to eliminate the effect of MT depolymerization. For example, we show here (Figures S2N and S2O) that MT destabilization enhances KCl–induced insulin secretion only after low glucose pre-incubation, but not after pre-incubation in stimulatory glucose.

Overall, our findings have important implications for the understanding of β-cell function and dysfunction. Importantly, we found that β-cell MTs restrict GSIS in mice, indicating that the rheostat mechanism is likely active in organisms. Dysfunctional β cells in diabetic mice have abnormally high MT density; moreover, the MT networks of murine and human β cells are remodeled by glucose similarly, suggesting a general MT-dependent function relevant to human β-cell physiology. In light of our data, several already FDA-approved MT-targeting anticancer drugs (Perez, 2009) might be considered as possible therapeutic interventions for diabetes.

EXPERIMENTAL PROCEDURES

Mice utilization followed protocols approved by the Vanderbilt Institutional Animal Care and Use Committee (IACUC). Most studies utilize islets from WT mice with mixed genetic background. *Rip*^{mCherry} mice were derived by pronuclear injection, with a 0.7 kb rat *Insulin 2* promoter (Postic et al., 1999) driving mCherry-insulin expression. The 10 week C57BL/KsJ *db/db* mice and their littermates that were used to compare MT organization were from Jackson Laboratory. Staining of sections and islets followed published protocols (Matsuoka et al., 2010; Wang et al., 2008). Pancreatic islets were handpicked after in situ collagenase perfusion and digestion. Human islets were from the Integrated Islet Distribution Program. RPE1 and INS-1 832/13 cells were cultured as previously described (Efimov et al., 2007; Hohmeier et al., 2000). The flattened islets were used after more than 1 week, but less than 2 weeks in culture, during which, the cultured islets maintain robust GSIS: insulin secretion (in % of total insulin content) in flattened islets was 0.03 ± 0.0026% (basal) and 0.6 ± 0.0014% (stimulated), as compared to 0.02 ± 3.8 × E^{-05}% (basal) /0.62 ± 0.001% (stimulated) in freshly isolated islets (n = 4).

Islet perifusion and static GSIS assay were carried out as previously described (Dai et al., 2012; Zhao et al., 2010). For perifusion, nocodazole (5 μg/ml) was added simultaneously with glucose stimulation. For static GSIS assay, nocodazole (10 μg/ml) or taxol (10 μM) were added to the pre-incubation buffer and present throughout the experiments.

For immunofluorescence, islets were fixed with 4% paraformaldehyde. Tissue culture cells were fixed with methanol at −20°C. Immunofluorescence followed described protocol (Mourad et al., 2011). 3D images were then captured with a Leica TCS5p or DeltaVision OMX.

For live-cell imaging of MT dynamics, INS-1 cells were transfected with GFP-centrin (centrosome), RFP-TGN (Golgi), GFP-EB3 (MT plus-end), and imaged in 3 mM or 20 mM glucose by spinning disk confocal imaging system described previously (Efimov et al., 2007). For insulin dynamics, flattened islets from *Rip*^{mCherry}-mice were imaged in the presence of 2.8 mM or 20 mM glucose by TIRF microscopy as described previously (Efimov et al., 2008). To detect insulin secretion after glucose stimulation by FluoZin-3 (Gee et al., 2002) (Figures 2C–2F and Movie S4), flattened islets were prepared and pre-incubated with nocodazole or DMSO. Glucose and FluoZin-3 in Kreb's Ringer Buffer (KRB) buffer were added to the sample on the microscope stage to final concentrations of 20 mM glucose and 20 μM Fluozin-3.

For MT regrowth after nocodazole washout, nocodazole was applied to fully disassemble MTs and then washed out to allow for MT repolymerization.

For all fluorescence images presented, brightness, contrast, and gamma settings for each individual fluorescence channel were adjusted to make small structural features visible. Image analysis was done with Image J, Imaris, and MatLab.

All the statistics were performed with MatLab software. All quantitative data were collected from experiments performed in at least triplicate and expressed as mean ± SEM. For data sets characterized by normal distribution, F-test was performed to test for the equal variance, followed by t test. For data sets, which did not follow normal distribution, Wilcoxon tests were performed to test the statistical difference between the two groups. For categorical data (Figures 3E and 5K), chi-square test was performed. For the correlation between total insulin content and IEQ, regression analysis was performed. Differences were considered significant when $p < 0.05$.

SUPPLEMENTAL INFORMATION

Supplemental Information includes Supplemental Experimental Procedures, four figures, two tables, and eight movies and can be found with this article online at http://dx.doi.org/10.1016/j.devcel.2015.08.020.

AUTHOR CONTRIBUTIONS

I.K. and G.G. conceived the project, designed the experiments, and wrote the paper. M.B. and A.C.P. designed and supervised experiments with human islets and islet perifusion assays and edited the manuscript. X.Z. designed the experiments and analyzed the data. X.Z. and R.H. performed the majority of the experiments. R.W.S. supervised the *db*/*db* mice experiments. All authors provided intellectual input, and vetted and approved the final manuscript.

ACKNOWLEDGMENTS

This work is supported by a P&F grant (to I.K.) from, and utilized the core(s) of, the Vanderbilt Diabetes Research and Training Center funded by grant DK020593 from the National Institute of Diabetes and Digestive and Kidney Diseases (NIDDK). Other support includes: NIH grant GM078373 (to I.K.); DK65949 (to G.G.); DK50203 and DK90570 (to R.W.S.); DK69603, DK72473, DK89572, DK89538, DK094199, and DK097829 (to A.C.P.); CA68485, DK58404, and DK59637 (to the Vanderbilt University Cell Imaging Shared Resource); American Heart Association grant-in-aid 13GRNT16980096 (to I.K.); grant from the Department of Veterans Affairs BX000666 (to A.C.P.); and Juvenile Diabetes Research Foundation (JDRF) grants 1-2009-371 (to G.G.) and 5-2011-379 (to A.C.P.). Islet isolation and perifusion were performed in the Vanderbilt Islet Procurement and Analysis Core supported by the Vanderbilt DRTC (DK20593). The authors thank the IIDP (https://iidp.coh.org) for human islets. The authors also thank Drs. Christopher Wright, Ian Macara, William Tansey, Matthew Tyska, David Piston, and Ryoma Ohi for suggestions and critical reading of the manuscript.

Received: April 11, 2015
Revised: June 4, 2015
Accepted: August 26, 2015
Published: September 28, 2015

REFERENCES

Alberts, B., Johnson, A., Lewis, J., Raff, M., Roberts, K., and Perter, W. (2002). Molecular Biology of the Cell: The Self-Assembly and Dynamic Structure of Cytoskeletal Filaments (New York: Garland Science).

Ally, S., Larson, A.G., Barlan, K., Rice, S.E., and Gelfand, V.I. (2009). Opposite-polarity motors activate one another to trigger cargo transport in live cells. J. Cell Biol. *187*, 1071–1082.

Boyd, A.E., 3rd, Bolton, W.E., and Brinkley, B.R. (1982). Microtubules and beta cell function: effect of colchicine on microtubules and insulin secretion in vitro by mouse beta cells. J. Cell Biol. *92*, 425–434.

Bryantseva, S.A., and Zhapparova, O.N. (2012). Bidirectional transport of organelles: unity and struggle of opposing motors. Cell Biol. Int. *36*, 1–6.

Chang, Y.C., Nalbant, P., Birkenfeld, J., Chang, Z.F., and Bokoch, G.M. (2008). GEF-H1 couples nocodazole-induced microtubule disassembly to cell contractility via RhoA. Mol. Biol. Cell *19*, 2147–2153.

Cui, J., Wang, Z., Cheng, Q., Lin, R., Zhang, X.M., Leung, P.S., Copeland, N.G., Jenkins, N.A., Yao, K.M., and Huang, J.D. (2011). Targeted inactivation of kinesin-1 in pancreatic β-cells in vivo leads to insulin secretory deficiency. Diabetes *60*, 320–330.

Dai, C., Brissova, M., Hang, Y., Thompson, C., Poffenberger, G., Shostak, A., Chen, Z., Stein, R., and Powers, A.C. (2012). Islet-enriched gene expression and glucose-induced insulin secretion in human and mouse islets. Diabetologia *55*, 707–718.

Dean, P.M. (1973). Ultrastructural morphometry of the pancreatic -cell. Diabetologia *9*, 115–119.

Donelan, M.J., Morfini, G., Julyan, R., Sommers, S., Hays, L., Kajio, H., Briaud, I., Easom, R.A., Molkentin, J.D., Brady, S.T., and Rhodes, C.J. (2002). Ca2+-dependent dephosphorylation of kinesin heavy chain on beta-granules in pancreatic beta-cells. Implications for regulated beta-granule transport and insulin exocytosis. J. Biol. Chem. *277*, 24232–24242.

Efendic, S., and Portwood, N. (2004). Overview of incretin hormones. Horm. Metab. Res. *36*, 742–746.

Efimov, A., Kharitonov, A., Efimova, N., Loncarek, J., Miller, P.M., Andreyeva, N., Gleeson, P., Galjart, N., Maia, A.R., McLeod, I.X., et al. (2007). Asymmetric CLASP-dependent nucleation of noncentrosomal microtubules at the trans-Golgi network. Dev. Cell *12*, 917–930.

Efimov, A., Schiefermeier, N., Grigoriev, I., Ohi, R., Brown, M.C., Turner, C.E., Small, J.V., and Kaverina, I. (2008). Paxillin-dependent stimulation of microtubule catastrophes at focal adhesion sites. J. Cell Sci. *121*, 196–204.

Gee, K.R., Zhou, Z.L., Qian, W.J., and Kennedy, R. (2002). Detection and imaging of zinc secretion from pancreatic beta-cells using a new fluorescent zinc indicator. J. Am. Chem. Soc. *124*, 776–778.

Goode, B.L., Drubin, D.G., and Barnes, G. (2000). Functional cooperation between the microtubule and actin cytoskeletons. Curr. Opin. Cell Biol. *12*, 63–71.

Gundersen, G.G., Gomes, E.R., and Wen, Y. (2004). Cortical control of microtubule stability and polarization. Curr. Opin. Cell Biol. *16*, 106–112.

Heaslip, A.T., Nelson, S.R., Lombardo, A.T., Beck Previs, S., Armstrong, J., and Warshaw, D.M. (2014). Cytoskeletal dependence of insulin granule movement dynamics in INS-1 beta-cells in response to glucose. PLoS ONE *9*, e109082.

Hoboth, P., Müller, A., Ivanova, A., Mziaut, H., Dehghany, J., Sönmez, A., Lachnit, M., Meyer-Hermann, M., Kalaidzidis, Y., and Solimena, M. (2015). Aged insulin granules display reduced microtubule-dependent mobility and are disposed within actin-positive multigranular bodies. Proc. Natl. Acad. Sci. USA *112*, E667–E676.

Hohmeier, H.E., Mulder, H., Chen, G., Henkel-Rieger, R., Prentki, M., and Newgard, C.B. (2000). Isolation of INS-1-derived cell lines with robust ATP-sensitive K+ channel-dependent and -independent glucose-stimulated insulin secretion. Diabetes *49*, 424–430.

Howell, S.L., Hii, C.S., Shaikh, S., and Tyhurst, M. (1982). Effects of taxol and nocodazole on insulin secretion from isolated rat islets of Langerhans. Biosci. Rep. *2*, 795–801.

Janke, C., and Bulinski, J.C. (2011). Post-translational regulation of the microtubule cytoskeleton: mechanisms and functions. Nat. Rev. Mol. Cell Biol. *12*, 773–786.

Kalwat, M.A., and Thurmond, D.C. (2013). Signaling mechanisms of glucose-induced F-actin remodeling in pancreatic islet β cells. Exp. Mol. Med. *45*, e37.

Kanaani, J., Cianciaruso, C., Phelps, E.A., Pasquier, M., Brioudes, E., Billestrup, N., and Baekkeskov, S. (2015). Compartmentalization of GABA synthesis by GAD67 differs between pancreatic beta cells and neurons. PLoS ONE *10*, e0117130.

Lacy, P.E., Howell, S.L., Young, D.A., and Fink, C.J. (1968). New hypothesis of insulin secretion. Nature *219*, 1177–1179.

Li, G., Rungger-Brändle, E., Just, I., Jonas, J.C., Aktories, K., and Wollheim, C.B. (1994). Effect of disruption of actin filaments by Clostridium botulinum C2 toxin on insulin secretion in HIT-T15 cells and pancreatic islets. Mol. Biol. Cell *5*, 1199–1213.

Malaisse, W.J., Van Obberghen, E., Devis, G., Somers, G., and Ravazzola, M. (1974). Dynamics of insulin release and microtubular-microfilamentous system. V. A model for the phasic release of insulin. Eur. J. Clin. Invest. *4*, 313–318.

Marsh, B.J., Volkmann, N., McIntosh, J.R., and Howell, K.E. (2004). Direct continuities between cisternae at different levels of the Golgi complex in glucose-stimulated mouse islet beta cells. Proc. Natl. Acad. Sci. USA *101*, 5565–5570.

Matsuoka, T.A., Kaneto, H., Miyatsuka, T., Yamamoto, T., Yamamoto, K., Kato, K., Shimomura, I., Stein, R., and Matsuhisa, M. (2010). Regulation of MafA expression in pancreatic beta-cells in db/db mice with diabetes. Diabetes *59*, 1709–1720.

McDonald, A., Fogarty, S., Leclerc, I., Hill, E.V., Hardie, D.G., and Rutter, G.A. (2009). Control of insulin granule dynamics by AMPK dependent KLC1 phosphorylation. Islets *1*, 198–209.

Meng, Y.X., Wilson, G.W., Avery, M.C., Varden, C.H., and Balczon, R. (1997). Suppression of the expression of a pancreatic beta-cell form of the kinesin heavy chain by antisense oligonucleotides inhibits insulin secretion from primary cultures of mouse beta-cells. Endocrinology *138*, 1979–1987.

Mourad, N.I., Nenquin, M., and Henquin, J.C. (2011). Metabolic amplification of insulin secretion by glucose is independent of β-cell microtubules. Am. J. Physiol. Cell Physiol. *300*, C697–C706.

Olofsson, C.S., Göpel, S.O., Barg, S., Galvanovskis, J., Ma, X., Salehi, A., Rorsman, P., and Eliasson, L. (2002). Fast insulin secretion reflects exocytosis of docked granules in mouse pancreatic B-cells. Pflugers Arch. *444*, 43–51.

Orland, M.J., and Permutt, M.A. (1987). Quantitative analysis of pancreatic proinsulin mRNA in genetically diabetic (db/db) mice. Diabetes *36*, 341–347.

Perez, E.A. (2009). Microtubule inhibitors: Differentiating tubulin-inhibiting agents based on mechanisms of action, clinical activity, and resistance. Mol. Cancer Ther. *8*, 2086–2095.

Postic, C., Shiota, M., Niswender, K.D., Jetton, T.L., Chen, Y., Moates, J.M., Shelton, K.D., Lindner, J., Cherrington, A.D., and Magnuson, M.A. (1999). Dual roles for glucokinase in glucose homeostasis as determined by liver and pancreatic beta cell-specific gene knock-outs using Cre recombinase. J. Biol. Chem. *274*, 305–315.

Rorsman, P., and Renström, E. (2003). Insulin granule dynamics in pancreatic beta cells. Diabetologia *46*, 1029–1045.

Saxton, M.J. (2007). A biological interpretation of transient anomalous subdiffusion. I. Qualitative model. Biophys. J. *92*, 1178–1191.

Semenova, I., Burakov, A., Berardone, N., Zaliapin, I., Slepchenko, B., Svitkina, T., Kashina, A., and Rodionov, V. (2008). Actin dynamics is essential for myosin-based transport of membrane organelles. Curr. Biol. *18*, 1581–1586.

Sharp, G.W. (1979). The adenylate cyclase-cyclic AMP system in islets of Langerhans and its role in the control of insulin release. Diabetologia *16*, 287–296.

Sumara, G., Formentini, I., Collins, S., Sumara, I., Windak, R., Bodenmiller, B., Ramracheya, R., Caille, D., Jiang, H., Platt, K.A., et al. (2009). Regulation of PKD by the MAPK p38delta in insulin secretion and glucose homeostasis. Cell *136*, 235–248.

Suprenant, K.A., and Dentler, W.L. (1982). Association between endocrine pancreatic secretory granules and in-vitro-assembled microtubules is dependent upon microtubule-associated proteins. J. Cell Biol. *93*, 164–174.

Tabei, S.M., Burov, S., Kim, H.Y., Kuznetsov, A., Huynh, T., Jureller, J., Philipson, L.H., Dinner, A.R., and Scherer, N.F. (2013). Intracellular transport of insulin granules is a subordinated random walk. Proc. Natl. Acad. Sci. USA *110*, 4911–4916.

Thurmond, D.C., Gonelle-Gispert, C., Furukawa, M., Halban, P.A., and Pessin, J.E. (2003). Glucose-stimulated insulin secretion is coupled to the interaction of actin with the t-SNARE (target membrane soluble N-ethylmaleimide-sensitive factor attachment protein receptor protein) complex. Mol. Endocrinol. *17*, 732–742.

Tsuboi, T., and Rutter, G.A. (2003). Insulin secretion by 'kiss-and-run' exocytosis in clonal pancreatic islet beta-cells. Biochem. Soc. Trans. *31*, 833–836.

Varadi, A., Ainscow, E.K., Allan, V.J., and Rutter, G.A. (2002). Involvement of conventional kinesin in glucose-stimulated secretory granule movements and exocytosis in clonal pancreatic beta-cells. J. Cell Sci. *115*, 4177–4189.

Varadi, A., Tsuboi, T., Johnson-Cadwell, L.I., Allan, V.J., and Rutter, G.A. (2003). Kinesin I and cytoplasmic dynein orchestrate glucose-stimulated insulin-containing vesicle movements in clonal MIN6 beta-cells. Biochem. Biophys. Res. Commun. *311*, 272–282.

Wang, Z., and Thurmond, D.C. (2009). Mechanisms of biphasic insulin-granule exocytosis - roles of the cytoskeleton, small GTPases and SNARE proteins. J. Cell Sci. *122*, 893–903.

Wang, S., Hecksher-Sorensen, J., Xu, Y., Zhao, A., Dor, Y., Rosenberg, L., Serup, P., and Gu, G. (2008). Myt1 and Ngn3 form a feed-forward expression loop to promote endocrine islet cell differentiation. Dev. Biol. *317*, 531–540.

Wollheim, C.B., and Sharp, G.W. (1981). Regulation of insulin release by calcium. Physiol. Rev. *61*, 914–973.

Wu, X., Bowers, B., Rao, K., Wei, Q., and Hammer, J.A., 3rd (1998). Visualization of melanosome dynamics within wild-type and dilute melanocytes suggests a paradigm for myosin V function In vivo. J. Cell Biol. *143*, 1899–1918.

Zhao, A., Ohara-Imaizumi, M., Brissova, M., Benninger, R.K., Xu, Y., Hao, Y., Abramowitz, J., Boulay, G., Powers, A.C., Piston, D., et al. (2010). Gαo represses insulin secretion by reducing vesicular docking in pancreatic beta-cells. Diabetes *59*, 2522–2529.